

Nonequilibrium Universality of a Squeezing Phase Transition

Arman Duha,¹ Samuel E. Begg,¹ and Thomas Bilitewski^{1,*}

¹*Department of Physics, Oklahoma State University, Stillwater, Oklahoma 74078, USA*

(Dated: April 2, 2025)

We investigate phase transitions in the nonequilibrium dynamics of power-law interacting spin-1/2 bilayer XXZ models, which have recently been shown to allow generation of entanglement in the form of two-mode squeezing. We find a transition between a phase characterized by Heisenberg limited squeezing and a partially collective phase. We identify universal scaling of the squeezing dynamics in terms of system parameters and a divergent time-scale, establishing these as distinct dynamical phases. Our work demonstrates a novel dynamical phase transition with potential applications in quantum sensing and quantum simulation in cold-atomic, molecular or Rydberg platforms.

Introduction—Matter in equilibrium can be classified into phases characterized by universal behavior irrespective of microscopic details [1–4], which facilitates understanding of large classes of systems. Similarly, the dynamics of systems out-of-equilibrium can present universal properties [4–6] allowing a classification of non-equilibrium phases of matter [7, 8]. This is well understood in the classical case, with paradigmatic examples such as flocking [9–11], Kardar-Parisi-Zhang physics [12], aging [13], and directed percolation [7]. More recently, nonequilibrium universality has been established in quantum systems, e.g. in the form of dynamical quantum phase transitions [14–17], measurement-induced phase transitions [18, 19], and in pre-thermal and driven phases of matter [20–22].

An important nonequilibrium process [23] is the generation of useful highly entangled states for quantum metrology [24–26] via time evolution from simple, easy to prepare, initial states. This includes the preparation of spin-squeezed states [27–29] with spin projection noise below the standard quantum limit, which facilitates quantum enhanced sensing. Spin squeezing has been predicted to occur in power law interacting spin systems [30–34], which was recently demonstrated in a number of experiments [35–38]. The wide range of experimental platforms realizing long-range interactions [39], from Rydberg [40–42] and magnetic atoms [43], over polar molecules [44–46] and trapped ions [47, 48], to cavity systems [49–51], makes these systems particularly promising candidates to controllably investigate many-body nonequilibrium dynamics and entanglement generation.

A natural question is whether the dynamical preparation of highly entangled squeezed states can be understood through the lens of phases and universality. Recent works have made progress in this direction by demonstrating that spin squeezing can be related to equilibrium phases of matter [33, 34]. Specifically, Block et al. [33] showed that quenches of quantum magnets that thermalize to temperatures within the easy plane ferromagnetic phase

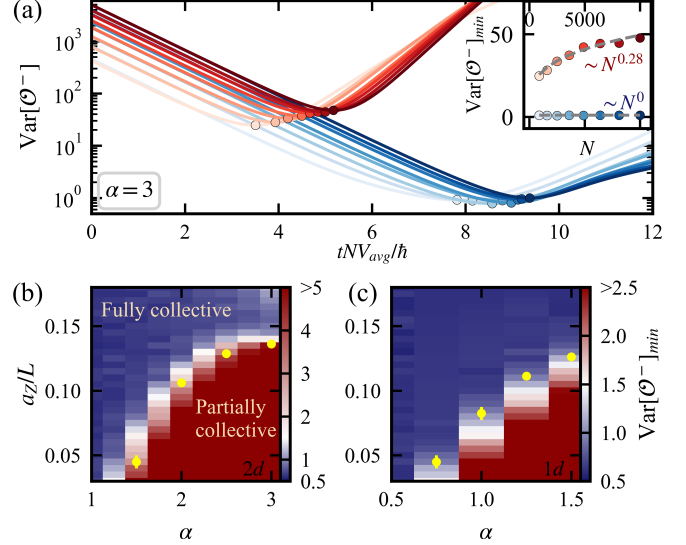


FIG. 1. Dynamical phases of squeezing. (a) Time evolution of the variance of the squeezed quadrature $\text{Var}[\hat{O}^-]$ in the fully collective regime (blue, $a_z/L = 0.17$) and partially collective regime (red, $a_z/L = 0.04$) for $\alpha = 3$ in $2d$. The opacity increases with system size $N \in \{9 \times 10^2, 10^4\}$. Inset: System size scaling of the minimum variance $\text{Var}[\hat{O}^-]_{\min}$ defining the fully, $\text{Var}[\hat{O}^-]_{\min} \sim N^0$, and partially collective regime $\sim N^{0.28}$. (b, c) Dynamical phase diagram as a function of power law exponent α and aspect ratio a_z/L in (b) $2d$ and (c) $1d$. The fully collective regime spans all a_z/L for $\alpha \leq d/2$, whereas a transition occurs at a critical a_z/L value (yellow marker) when $\alpha > d/2$.

can exhibit scalable squeezing in their time dynamics. It was then shown that a similar picture emerges even in the case of short-range interacting systems with only quasi-long-range order [34], with critical slowing down protecting scalable squeezing.

Here, we demonstrate non-equilibrium universality in the full time dynamics of a spin system that exhibits two mode squeezing. We first establish distinct dynamical regimes in terms of the scaling of the squeezing with system size. We then demonstrate the phenomenology of universality by resolving critical exponents governing the scaling with system-size and divergent time-scales as a

* thomas.bilitewski@okstate.edu

function of control parameters. This directly connects the observed system size scaling of squeezing to the universal scaling behavior within the corresponding dynamical phase.

Model—We consider power law interacting spin 1/2 systems in ladders (1d) or square bi-layers (2d) described by

$$\hat{H} = 1/2 \sum_{\eta} \sum_{i,j \in \eta} V_{ij} \vec{s}_i \cdot \vec{s}_j + \sum_{i \in A, j \in B} V_{ij} (\hat{s}_i^x \hat{s}_j^x + \hat{s}_i^y \hat{s}_j^y) \quad (1)$$

where the spin operators $\hat{s}_i^{\mu} = \hat{\sigma}_i^{\mu}/2$, with the Pauli matrices $\hat{\sigma}^{\mu}$, act on the spin at site i , specifying the position in layers (denoted by $\eta = A, B$) of a one-dimensional spin-ladder or a two-dimensional bi-layer.

The chains or layers are separated by a distance a_Z , which we measure in terms of the in-layer spacing a_{lat} , set to 1 in the following. We choose power-law interactions with exponent α of the form $V_{ij} = |\mathbf{r}_i - \mathbf{r}_j|^{-\alpha}$, modeling a range of experimental platforms [39] from Rydberg atoms [40–42], polar molecules [44–46], magnetic atoms [43], trapped ions [47, 48], or cavity systems [49–51]. Recent work [32] has shown that the spin structure of the interactions in Eq. 1 can be obtained starting from pure Ising interactions using Floquet engineering techniques.

We initialize non-equilibrium dynamics starting from an initial state of oppositely polarized layers, $\langle \hat{S}_A \rangle = -\langle \hat{S}_B \rangle = N/2 \hat{z}$. We note that this initial state is an infinite temperature state of the inter-layer interactions, and thus would not show equilibrium order. The interlayer spin-exchange interactions, second term of Eq. 1, will dynamically create entangled pairs of excitations and two-mode squeezing [32, 52, 53]. To see this, one can perform a Holstein-Primakoff transformation [54] of the total layer spins to obtain $H \approx NV_{\text{avg}}(\hat{a}^{\dagger} \hat{b}^{\dagger} + \hat{a} \hat{b})/2$, the two-mode squeezing Hamiltonian [55–57], where V_{avg} is the average interlayer interaction and \hat{a} (\hat{b}) describes excitations in layer A (B). This predicts exponential growth/decay of variances $\text{Var}[\mathcal{O}^{\pm}] = N/2 e^{\pm NV_{\text{avg}} t/\hbar}$, i.e. squeezing of $\mathcal{O}^{-} = S_A^x + S_B^y$ or $S_A^y - S_B^x$, and anti-squeezing of $\mathcal{O}^{+} = S_A^x - S_B^y$ or $S_A^y + S_B^x$.

Dynamical transitions in spin squeezing—We now explore the dynamical regimes of the model Eq. 1 as a function of the dimensionality of the system d , power-law exponents of the interactions α , and aspect ratio a_Z/L . To simulate the full quantum many-body nonequilibrium dynamics we use the discrete truncated Wigner approximation (dTWA) [58–60] for up to $2N = 2 \times 100^2 = 20000$ spins in 2d and $2N = 2 \times 2500 = 5000$ spins in 1d.

Our main results are summarized in Fig. 1. In Fig. 1(a) we show the time evolution of the variance of the squeezed quadratures, $\text{Var}[\mathcal{O}^{-}]$, for the representative case of $\alpha = 3$ with $a_Z/L = 0.04$ (red) and $a_Z/L = 0.17$ (blue). Our results show that in both cases the spin dynamics follow the two-mode squeezing prediction of exponentially

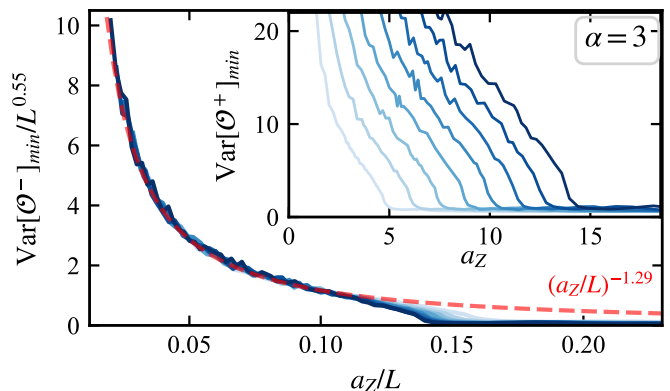


FIG. 2. Universal scaling collapse of minimal squeezing. Inset: Dependence of minimal variance $\text{Var}[\mathcal{O}^{-}]_{\text{min}}$ on layer spacing a_Z , for different system sizes ($L = 30$ to 100) with $\alpha = 3$ in 2d. The opacity increases with system size. Main panel: Rescaled minimal variance $\text{Var}[\mathcal{O}^{-}]_{\text{min}}/L^{0.55}$ versus aspect ratio a_Z/L for the same system sizes, demonstrating a universal collapse onto a single curve. Red dashed line power-law $(a_Z/L)^{-1.29}$ obtained from the scaling ansatz, Eq. 3.

decreasing variance up to a saturation point of minimal variance. Results are shown for a range of system sizes (faded lines), and indicate that for the larger (smaller) a_Z/L value this minimum does not (does) depend on the system size. This is shown directly in the inset of Fig. 1(a) where we plot the minimum variance $\text{Var}[\mathcal{O}^{-}]_{\text{min}}$ vs N . The results for smaller a_Z/L approximately follow $\text{Var}[\mathcal{O}^{-}]_{\text{min}} \sim N^p$ with $p = 0.28$, whereas the larger a_Z/L data exhibits $p = 0$. This suggests the presence of two dynamical regimes: a partially collective regime (red) with $p > 0$ and a fully collective regime (blue) with $p = 0$.

We map out these two dynamical regimes in Fig. 1(b) and (c) as a function of the aspect ratio a_Z/L and power-law exponents α for 1d (b) and 2d (c). For $\alpha > d/2$, a critical a_Z/L exists (white), above which the value of minimal variance remains constant around ~ 1 (blue), signifying the fully collective behavior of this regime. On the contrary, below these critical values the minimal variance is greater than $\mathcal{O}(1)$ and scales with system size, marking the departure from the fully collective regime into a partially collective regime. The dynamics remain fully collective if $\alpha \leq d/2$. We identify the critical $(a_Z/L)_*$ values marked by yellow markers in Fig. 1 (b) and (c) via the scaling of the minimum variance with system size. In the fully collective regime, the minimal variance shows no scaling, $\text{Var}[\mathcal{O}^{-}]_{\text{min}} \sim N^p$, with $p = 0$. The advent of system size scaling $p > 0$ indicates the departure from this fully collective region and thus the critical $(a_Z/L)_*$ is defined by the point at which the scaling exponent becomes non-zero, see Fig. S2 of the supplemental material (SM) [61].

The role of the aspect ratio a_Z/L as a control parameter can be understood in terms of the spatial inhomogeneity of the interlayer interactions. Systems with larger L re-

quire larger layer separation a_z to maintain sufficiently homogeneous interlayer interactions to remain in the collective manifold. Consequently, the critical a_z values at which the transition occurs is expected to increase with L , which is captured by the ratio a_z/L .

Scaling of variance minima—We now confirm this intuition and demonstrate scaling of the minimal variance in the respective phases. The inset of Fig. 2 shows the minimal variance versus layer separation a_z for different system sizes in the $\alpha = 3$ case in $2d$, clearly showing that the critical a_z scales with L .

In the main panel of Fig. 2 we plot the data as a function of a_z/L , which then corresponds to a horizontal cut of the phase diagram in Fig. 1(b), and rescale the minimal variance by $L^{-0.55}$, noting that since $N = L^2$ in $2d$ this is equivalent to the $N^{0.28}$ scaling observed in the inset of Fig. 1(a). Under this rescaling the data collapses to a single curve, or scaling function, demonstrating that the aspect ratio a_z/L controls the transition, and that both distinct regimes show universal scaling of the minimal variance. Further, while finite size discrepancies near the critical value $(a_z/L)_* \approx 0.14$ are visible for smaller L , these are seen to vanish with increasing L .

The dashed line $(a_z/L)^{d_V}$ is an excellent fit to the scaling function, with $d_V = -1.29$ which we will later demonstrate to be a critical exponent. Details of the calculation of scaling exponents and data for other α in $1d$ and $2d$ can be found in the Supplemental Material (SM) [61].

Dependence of critical point on interaction inhomogeneity—We next provide a physical understanding of the transition in terms of a competition between the intra-layer interactions and the inter-layer interaction inhomogeneity. We define a control parameter $G = \sqrt{\text{Var}[V_{AB}]/V_{\eta\eta}^{\text{avg}}}$, where $\sqrt{\text{Var}[V_{AB}]}$ is the standard deviation of interlayer interactions, a measure of their inhomogeneity and departure from fully collective interactions, while $V_{\eta\eta}^{\text{avg}}$ is the average of the intralayer interactions. This is motivated by the understanding that given the fully collective initial state, an eigenstate of the intra-layer Heisenberg interactions, any non-collective excitations can only be created by inhomogeneous (non-collective) inter-layer interactions, a process which is energetically suppressed by the average intra-layer interactions.

In the main panel of Fig. 3 we plot the minimal variance versus G for $\alpha = 2$ in $2d$. This shows the appearance of a system size independent critical value G_* for the transition from fully collective to partially collective regimes. In the inset of Fig. 3, we plot the system size scaling exponent q of the minimal variance, $\text{Var}[\mathcal{O}^-]_{\min} \sim N^q$, as we vary G . A sharp transition from fully collective regime ($q = 0$) to partially collective regime ($q > 0$) is seen to occur at a critical $G = G_*$, consistent with the transition seen in the main panel. Similar universal transitions with respect to G are observed for all long-range ($\alpha \leq d$) interactions.

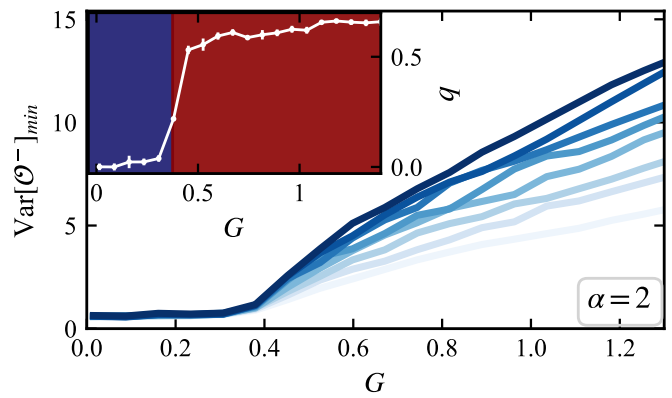


FIG. 3. Interaction inhomogeneity driven transition. Dependence of minimal variance $\text{Var}[\mathcal{O}^-]_{\min}$ on interaction inhomogeneity, G (see text), for different system sizes ($L = 30$ to 100) with $\alpha = 2$ in $2d$. The opacity increases with system size. Inset: Scaling exponent, q , of minimal variance ($\text{Var}[\mathcal{O}^-]_{\min} \sim L^q$) versus G . At a critical value of G , q changes from zero to a nonzero value, corresponding to the transition from fully collective to partially collective.

This indicates that our simple explanation underlying the transition holds in the strongly collective long-range regime. We note that this also implies a transition at a specific a_z/L . However, for short range interactions ($\alpha \geq d$), G_* is no longer independent of L , suggesting that the standard deviation $\sqrt{\text{Var}[V_{AB}]}$ as an incomplete measure of the spatial inhomogeneity cannot fully describe the transition out of the collective manifold.

Universality of the partially collective phase—Having demonstrated a clear transition between two regimes, quantified by the exponent p which plays the role of an order parameter, we now turn to establishing the partially collective regime as a proper phase in the sense that it shows universal scaling in the vicinity of a critical point, just as occurs for equilibrium phases.

Since the variance minima occur at different times t_{\min} that grow with increasing a_z , the scaling collapse in Fig. 2 is suggestive that the partially collective phase may obey a universal scaling that depends on a diverging relaxation time-scale, in analogy to critical slowing down at equilibrium transitions. We now show that the universality is captured by a system-size independent relation $\tilde{V} = f(\tau, a_{z,\delta})$, where $\tau = (t - t_{\min})$ and we have assumed the system-size dependence is removed by using the system size independent variance $\tilde{V} = N^{-\nu} \text{Var}[\mathcal{O}^-]$. We also define the scaled layer spacing $a_{z,\delta} = L^{-\delta} a_z$, where the exponent δ determines how a_z should be scaled to compensate for changes of the layer length scale $L = N^{1/d}$. We then use basic scaling theory [62] to arrive at the scaling ansatz

$$\text{Var}[\mathcal{O}^-] a_z^{-d_V} N^{d_V \delta / d - \nu} = f[(t - t_{\min}) a_z^{-d_\tau} N^{\delta d_\tau / d}] \quad (2)$$

The new exponents d_V and d_τ characterize the divergence of \tilde{V} and t , respectively, with $a_{z,\delta}$. To demonstrate the

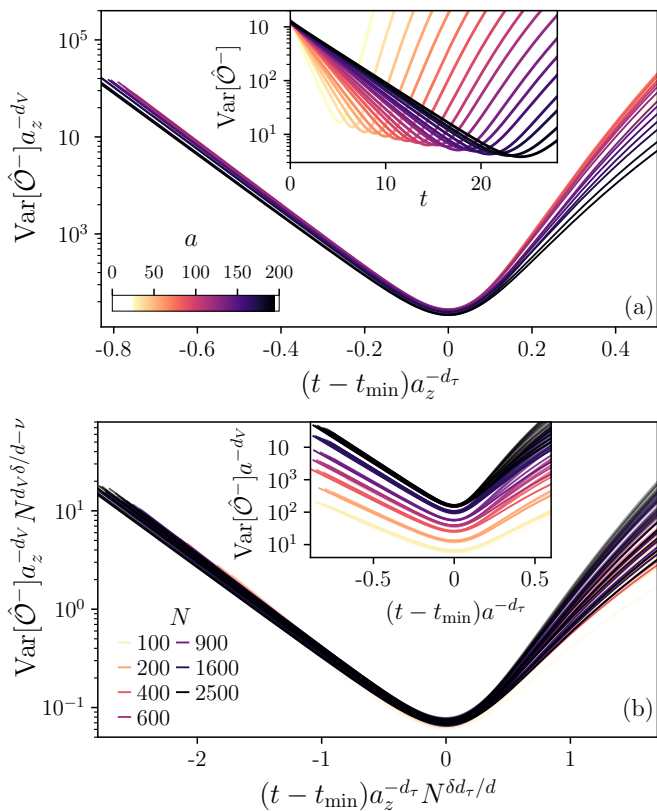


FIG. 4. Universality of the partially collective phase. (a) $\text{Var}[\hat{\mathcal{O}}^-] a_z^{-d_V}$ vs rescaled time $t a_z^{-d_T}$ for different a_z values in the partially collective regime (colorbar). Inset: raw data $\text{Var}[\hat{\mathcal{O}}^-]$ vs time t for a 1d system with $\alpha = 1.5$. (b) Same as in (a) but for a range of system sizes (legend) and with additional system size rescaling, giving variance $\text{Var}[\hat{\mathcal{O}}^-] N^{-\nu} a_{z,\delta}^{-d_V}$ vs rescaled time $(t - t_{\min}) a_{z,\delta}^{-d_T}$. For each N , a range of a_z values are plotted with increased fading for smaller values. Inset: data without N rescaling. The exponents are $d_T = 0.63$, $d_V = -0.69$, $\nu = 0.81$ and $\delta = 0.25$.

efficacy of the ansatz let us first consider the simpler case where the system size N is fixed. This allows N to be absorbed into the scaling function, now f_N , and the ansatz reduces to $\text{Var}[\hat{\mathcal{O}}^-] a_z^{-d_V} = f_N[(t - t_{\min}) a_z^{-d_T}]$. To demonstrate this scaling, Fig. 4(a) shows $\text{Var}[\hat{\mathcal{O}}^-] a_z^{-d_V}$ vs $(t - t_{\min}) a_z^{-d_T}$ for a variety of a_z values. The data corresponds to the case of $\alpha = 1.5$ with $d = 1$, for which we can reach large enough system sizes to simulate an order of magnitude of a_z values in the partially collective phase [63]. While the raw data varies substantially with a_z (inset), the scaled data collapse to a single curve f_N up until $t \sim t_{\min}$, after which point additional interaction effects are anticipated to become substantial.

The inset of Fig. 4(b) shows the aforementioned f_N for a variety of N (colors). To demonstrate the full scaling collapse according to Eq. 2, in the main window we further scale both axes by the N -dependent terms in Eq 2, thereby demonstrating a complete collapse of the data across t ,

a_z and N . The exponents correspond to $d_T = 0.63(7)$, $d_V = -0.69(20)$, $\nu = 0.81(29)$ and $\delta = 0.25(4)$. In the SM [61] we demonstrate that the scaling collapse occurs for other α values in 1d, and for the accessible system sizes in 2d.

Finally, we clarify how the exponents relate to the scaling of variance minima considered in Fig. 2. In this case $t = t_{\min}$, which reduces the rhs of Eq. 2 to $f(0)$. Re-arranging the remaining terms, the expression can be placed in the form

$$\text{Var}[\hat{\mathcal{O}}^-]_{\min} N^{-p} = y(a_z/L), \quad (3)$$

where $y(x) = f(0)x^{d_V}$ and $p = d_V(1 - \delta)/d + \nu$. This reveals that the scaling function x^{d_V} shown in Fig. 2 itself contains universal information. Due to the simple form of $y(x)$, powers of N can be moved from the lhs of the Eq. 3 to the right. This emphasizes that while the naive aspect ratio a_z/L characterizes the critical point itself, as shown in Fig. 2, it is not of fundamental importance in the partially collective phase, with δ capturing the relevant scaling of a_z with system size. Intuitively, if $\alpha < d$ such that the interactions are genuinely long-ranged, then $\delta > 1$ ensures that as the system size increases the range of a_z values below the critical value $(a_z/L)_* = \text{constant}$ reduces, i.e. the system becomes more collective for larger L and it becomes difficult to observe the partially collective phase.

Outlook—Our work establishes nonequilibrium universality in the two-mode squeezing dynamics of powerlaw interacting spin ladders and bi-layers. Specifically, we find two dynamical squeezing phases, a fully collective phase and a partially collective phase, distinguished by the scaling of the achievable minimal variance. The transition between them is controlled by the layer aspect ratio a_z/L and the powerlaw exponent α . For $\alpha < d/2$ the system is always collective, whereas for $\alpha > d/2$ there is a transition at a finite a_z/L . Critically, we establish here universality of the full finite time dynamics in the partially collective phase in terms of a scaling ansatz, which also determines the scaling form of the minimal variance. This establishes that these regimes can be regarded as true dynamical phases, and the variance scaling exponent as an indicator of the phase transition.

Our work also establishes that scalable two mode squeezing can be realized with powerlaw interactions, even if the simplest implementation using single-layer two-axis twisting does not achieve scalable squeezing. We also demonstrate (Fig. S2 [61]) that scalable squeezing persists at fixed layer separation. This resolves the outstanding fundamental question of whether scalable squeezing is possible beyond the one-axis twisting paradigm in long-range [33] or quasi-long range [34] ordered phases.

It may also be interesting to connect the universality found here with that observed in short-range Heisenberg models [64]. While our analysis has identified a diverging time-scale as a function of the scaled layer separation $a_{z,\delta}$, our work focused on $\text{Var}[\hat{\mathcal{O}}^-]$ as a global quantity, from

which a correlation length can not simply be obtained, and other observables may need to be considered to address this.

Acknowledgements: The computing for this project was performed at the High Performance Computing Center at Oklahoma State University supported in part through the National Science Foundation grant OAC-1531128.

-
- [1] J. Zinn-Justin, *Quantum field theory and critical phenomena*, 4th ed., International Series of Monographs on Physics (Clarendon Press, Oxford, England, 2002).
- [2] N. Goldenfeld, *Lectures on phase transitions and the renormalization group* (CRC Press, London, England, 2019).
- [3] P. C. Hohenberg and B. I. Halperin, Theory of dynamic critical phenomena, *Rev. Mod. Phys.* **49**, 435 (1977).
- [4] U. C. Täuber, *Critical Dynamics: A Field Theory Approach to Equilibrium and Non-Equilibrium Scaling Behavior* (Cambridge University Press, 2014).
- [5] S. Lübeck, Universal scaling behavior of non-equilibrium phase transitions, *International Journal of Modern Physics B* **18**, 3977–4118 (2004).
- [6] J. Berges, K. Boguslavski, S. Schlichting, and R. Venugopalan, Universality far from equilibrium: From superfluid bose gases to heavy-ion collisions, *Phys. Rev. Lett.* **114**, 061601 (2015).
- [7] H. Hinrichsen, Non-equilibrium critical phenomena and phase transitions into absorbing states, *Advances in Physics* **49**, 815–958 (2000).
- [8] G. Ódor, Universality classes in nonequilibrium lattice systems, *Reviews of Modern Physics* **76**, 663–724 (2004).
- [9] T. Vicsek, A. Czirók, E. Ben-Jacob, I. Cohen, and O. Shochet, Novel Type of Phase Transition in a System of Self-Driven Particles, *Phys. Rev. Lett.* **75**, 1226 (1995).
- [10] J. Toner and Y. Tu, Long-Range Order in a Two-Dimensional Dynamical XY Model: How Birds Fly Together, *Phys. Rev. Lett.* **75**, 4326 (1995).
- [11] B. Mahault, F. Ginelli, and H. Chaté, Quantitative Assessment of the Toner and Tu Theory of Polar Flocks, *Phys. Rev. Lett.* **123**, 218001 (2019).
- [12] M. Kardar, G. Parisi, and Y.-C. Zhang, Dynamic Scaling of Growing Interfaces, *Phys. Rev. Lett.* **56**, 889 (1986).
- [13] P. Calabrese and A. Gambassi, Ageing properties of critical systems, *J. Phys. A* **38**, R133 (2005).
- [14] R. Schützhold, M. Uhlmann, Y. Xu, and U. R. Fischer, Sweeping from the superfluid to the mott phase in the bose-hubbard model, *Phys. Rev. Lett.* **97**, 200601 (2006).
- [15] M. Heyl, A. Polkovnikov, and S. Kehrein, Dynamical Quantum Phase Transitions in the Transverse-Field Ising Model, *Phys. Rev. Lett.* **110**, 135704 (2013).
- [16] M. Heyl, Dynamical quantum phase transitions: A review, *Rep. Prog. Phys.* **81**, 054001 (2018).
- [17] B. Žunkovič, M. Heyl, M. Knap, and A. Silva, Dynamical Quantum Phase Transitions in Spin Chains with Long-Range Interactions: Merging Different Concepts of Nonequilibrium Criticality, *Phys. Rev. Lett.* **120**, 130601 (2018).
- [18] B. Skinner, J. Ruhman, and A. Nahum, Measurement-induced phase transitions in the dynamics of entanglement, *Phys. Rev. X* **9**, 031009 (2019).
- [19] Y. Li, X. Chen, and M. P. A. Fisher, Measurement-driven entanglement transition in hybrid quantum circuits, *Phys. Rev. B* **100** (2019).
- [20] D. V. Else, B. Bauer, and C. Nayak, Prethermal phases of matter protected by time-translation symmetry, *Phys. Rev. X* **7**, 011026 (2017).
- [21] F. Machado, D. V. Else, G. D. Kahanamoku-Meyer, C. Nayak, and N. Y. Yao, Long-range prethermal phases of nonequilibrium matter, *Phys. Rev. X* **10**, 011043 (2020).
- [22] L. M. Sieberer, M. Buchhold, J. Marino, and S. Diehl, Universality in driven open quantum matter (2023), [arXiv:2312.03073](https://arxiv.org/abs/2312.03073) [cond-mat.stat-mech].
- [23] A. Polkovnikov, K. Sengupta, A. Silva, and M. Vengalattore, Colloquium: Nonequilibrium dynamics of closed interacting quantum systems, *Rev. Mod. Phys.* **83**, 863 (2011).
- [24] C. L. Degen, F. Reinhard, and P. Cappellaro, Quantum sensing, *Rev. Mod. Phys.* **89**, 035002 (2017).
- [25] L. Pezzè, A. Smerzi, M. K. Oberthaler, R. Schmied, and P. Treutlein, Quantum metrology with nonclassical states of atomic ensembles, *Rev. Mod. Phys.* **90**, 035005 (2018).
- [26] V. Montenegro, C. Mukhopadhyay, R. Yousefjani, S. Sarkar, U. Mishra, M. G. A. Paris, and A. Bayat, Review: Quantum metrology and sensing with many-body systems (2024), [arXiv:2408.15323](https://arxiv.org/abs/2408.15323) [quant-ph].
- [27] D. J. Wineland, J. J. Bollinger, W. M. Itano, F. L. Moore, and D. J. Heinzen, Spin squeezing and reduced quantum noise in spectroscopy, *Phys. Rev. A* **46**, R6797 (1992).
- [28] D. J. Wineland, J. J. Bollinger, W. M. Itano, and D. J. Heinzen, Squeezed atomic states and projection noise in spectroscopy, *Phys. Rev. A* **50**, 67 (1994).
- [29] M. Kitagawa and M. Ueda, Squeezed spin states, *Phys. Rev. A* **47**, 5138 (1993).
- [30] M. Foss-Feig, Z.-X. Gong, A. V. Gorshkov, and C. W. Clark, Entanglement and spin-squeezing without infinite-range interactions (2016), [arXiv:1612.07805](https://arxiv.org/abs/1612.07805) [cond-mat.quant-gas].
- [31] M. A. Perlin, C. Qu, and A. M. Rey, Spin squeezing with short-range spin-exchange interactions, *Phys. Rev. Lett.* **125**, 223401 (2020).
- [32] A. Duha and T. Bilitewski, Two-mode squeezing in floquet-engineered power-law interacting spin models, *Phys. Rev. A* **109**, L061304 (2024).
- [33] M. Block, B. Ye, B. Roberts, S. Chern, W. Wu, Z. Wang, L. Pollet, E. J. Davis, B. I. Halperin, and N. Y. Yao, Scalable spin squeezing from finite-temperature easy-plane magnetism, *Nat. Physics* **20**, 1575–1581 (2024).
- [34] T. Roscilde, F. Caleca, A. Angelone, and F. Mezzacapo, Scalable Spin Squeezing from Critical Slowing Down in Short-Range Interacting Systems, *Phys. Rev. Lett.* **133**, 210401 (2024).
- [35] W. J. Eckner, N. Darkwah Oppong, A. Cao, A. W. Young, W. R. Milner, J. M. Robinson, J. Ye, and A. M. Kaufman, Realizing spin squeezing with rydberg interactions in an optical clock, *Nature* **621**, 734–739 (2023).
- [36] J. Franke, S. R. Muleady, R. Kaubruegger, F. Kranzl, R. Blatt, A. M. Rey, M. K. Joshi, and C. F. Roos, Quantum-enhanced sensing on optical transitions through finite-range interactions, *Nature* **621**, 740 (2023).
- [37] G. Bornet, G. Emperauger, C. Chen, B. Ye, M. Block, M. Bintz, J. A. Boyd, D. Barredo, T. Comparin, F. Mezzacapo, T. Roscilde, T. Lahaye, N. Y. Yao, and A. Browaeys, Scalable spin squeezing in a dipolar rydberg atom array,

- Nature* **621**, 728 (2023).
- [38] J. A. Hines, S. V. Rajagopal, G. L. Moreau, M. D. Wahrman, N. A. Lewis, O. Marković, and M. Schleier-Smith, Spin squeezing by rydberg dressing in an array of atomic ensembles, *Phys. Rev. Lett.* **131**, 063401 (2023).
- [39] N. Defenu, T. Donner, T. Macrì, G. Pagano, S. Ruffo, and A. Trombettoni, Long-range interacting quantum systems, *Rev. Mod. Phys.* **95**, 035002 (2023).
- [40] A. Browaeys and T. Lahaye, Many-body physics with individually controlled rydberg atoms, *Nat. Physics* **16**, 132 (2020).
- [41] M. Saffman, T. G. Walker, and K. Mølmer, Quantum information with rydberg atoms, *Rev. Mod. Phys.* **82**, 2313 (2010).
- [42] M. Morgado and S. Whitlock, Quantum simulation and computing with rydberg-interacting qubits, *AVS Quantum Science* **3** (2021).
- [43] L. Chomaz, I. Ferrier-Barbut, F. Ferlaino, B. Laburthe-Tolra, B. L. Lev, and T. Pfau, Dipolar physics: a review of experiments with magnetic quantum gases, *Rep. Prog. Phys.* **86**, 026401 (2023).
- [44] M. A. Baranov, M. Dalmonte, G. Pupillo, and P. Zoller, Condensed matter theory of dipolar quantum gases, *Chemical Reviews* **112**, 5012 (2012).
- [45] J. L. Bohn, A. M. Rey, and J. Ye, Cold molecules: Progress in quantum engineering of chemistry and quantum matter, *Science* **357**, 1002 (2017).
- [46] S. A. Moses, J. P. Covey, M. T. Miecnikowski, D. S. Jin, and J. Ye, New frontiers for quantum gases of polar molecules, *Nat. Phys.* **13**, 13 (2017).
- [47] R. Blatt and C. F. Roos, Quantum simulations with trapped ions, *Nat. Physics* **8**, 277–284 (2012).
- [48] C. Monroe, W. C. Campbell, L.-M. Duan, Z.-X. Gong, A. V. Gorshkov, P. W. Hess, R. Islam, K. Kim, N. M. Linke, G. Pagano, P. Richerme, C. Senko, and N. Y. Yao, Programmable quantum simulations of spin systems with trapped ions, *Rev. Mod. Phys.* **93**, 025001 (2021).
- [49] M. A. Norcia, R. J. Lewis-Swan, J. R. K. Cline, B. Zhu, A. M. Rey, and J. K. Thompson, Cavity-mediated collective spin-exchange interactions in a strontium superradiant laser, *Science* **361**, 259–262 (2018).
- [50] E. J. Davis, G. Bentsen, L. Homeier, T. Li, and M. H. Schleier-Smith, Photon-mediated spin-exchange dynamics of spin-1 atoms, *Phys. Rev. Lett.* **122**, 010405 (2019).
- [51] T. D. Farokh Mivehvar, Francesco Piazza and H. Ritsch, Cavity qed with quantum gases: new paradigms in many-body physics, *Advances in Physics* **70**, 1 (2021).
- [52] T. Bilitewski and A. M. Rey, Manipulating growth and propagation of correlations in dipolar multilayers: From pair production to bosonic kitaev models, *Phys. Rev. Lett.* **131**, 053001 (2023).
- [53] T. Bilitewski, G. A. Domínguez-Castro, D. Wellnitz, A. M. Rey, and L. Santos, Tunable momentum pair creation of spin excitations in dipolar bilayers, *Phys. Rev. A* **108**, 013313 (2023).
- [54] T. Holstein and H. Primakoff, Field dependence of the intrinsic domain magnetization of a ferromagnet, *Physical Review* **58**, 1098 (1940).
- [55] G. Agarwal, *Quantum Optics*, Quantum Optics (Cambridge University Press, 2013).
- [56] B. L. Schumaker and C. M. Caves, New formalism for two-photon quantum optics. II. mathematical foundation and compact notation, *Phys. Rev. A* **31**, 3093 (1985).
- [57] C. M. Caves and B. L. Schumaker, New formalism for two-photon quantum optics. i. quadrature phases and squeezed states, *Phys. Rev. A* **31**, 3068 (1985).
- [58] J. Schachenmayer, A. Pikovski, and A. M. Rey, Many-body quantum spin dynamics with monte carlo trajectories on a discrete phase space, *Phys. Rev. X* **5**, 011022 (2015).
- [59] B. Zhu, A. M. Rey, and J. Schachenmayer, A generalized phase space approach for solving quantum spin dynamics, *New J. Phys.* **21**, 082001 (2019).
- [60] S. R. Muleady, M. Yang, S. R. White, and A. M. Rey, Validating phase-space methods with tensor networks in two-dimensional spin models with power-law interactions, *Phys. Rev. Lett.* **131**, 150401 (2023).
- [61] See Supplemental Material at [URL will be inserted by publisher], which includes Refs. [65, 66] for additional details on the optimization procedure used to estimate critical exponents, scaling analysis of the variance minima at fixed layer spacing, and additional examples of the scaling collapse figures shown in the main text for other power-law interaction exponents α and dimensions d .
- [62] A. Altland and B. D. Simons, *Condensed matter field theory*, 2nd ed. (Cambridge University Press, Cambridge, England, 2010).
- [63] Data in Figs. 4(a) and 4(b) is plotted for a_z values in the range $a_z/L \approx \{0.01, 0.078\}$. The critical exponents d_ν , d_τ and δ are extracted from data in the slightly smaller range $a_z/L \approx \{0.01, 0.07\}$ to reduce the proximity to the phase boundary shown in Fig. 1(c). The exponent ν is inferred from $\nu = p - d_\nu(1 - \delta)/d$. See Supplemental Material [61] for full details of the procedure.
- [64] J. F. Rodríguez-Nieva, A. Piñeiro Orioli, and J. Marino, Far-from-equilibrium universality in the two-dimensional heisenberg model, *Proceedings of the National Academy of Sciences* **119** (2022).
- [65] E. J. Dresselhaus, B. Sbierski, and I. A. Gruzberg, Scaling collapse of longitudinal conductance near the integer quantum hall transition, *Phys. Rev. Lett.* **129**, 026801 (2022).
- [66] J. Houdayer and A. K. Hartmann, Low-temperature behavior of two-dimensional gaussian ising spin glasses, *Phys. Rev. B* **70**, 014418 (2004).

Supplemental Material for “Nonequilibrium Universality of a Squeezing Phase Transition”

Arman Duha,¹ Samuel E. Begg,¹ and Thomas Bilitewski¹

¹*Department of Physics, Oklahoma State University, Stillwater, Oklahoma 74078, USA*

(Dated: April 2, 2025)

The Supplementary Material contains additional details on the optimization procedure used to estimate critical exponents, scaling analysis of the variance minima at fixed layer spacing, and additional examples of the scaling collapse figures shown in the main text for other power-law interaction exponents α and dimensions d .

Scaling of squeezing at fixed layer separation

So far we have looked at the system size dependency of minimal variance for the universal control parameters, a_Z/L and G , that illustrates the universality of the transition from fully collective to partially collective regimes. We now look at the scaling of minimal variance with system size for a fixed a_Z , which is more practical for systems with inherent difficulty varying the separation between two layers as the number of particles is increased. In Fig. S1 (a) we plot the scaling of minimal variance with system size for different power-law exponents α , represented by the color scheme of Fig. S1 (b), for the $2d$ case. As expected, the dynamics remain in the fully collective regime for $\alpha \leq d/2$. For $\alpha \geq d/2$, with increasing α as the interactions get weaker, the minimal variance shows stronger system size dependency before ultimately becoming linear to the system size at $\alpha = 3$, entering the fully non-collective regime. For the intermediate power-law exponents, $1 < \alpha < 3$, the sublinear scaling of minimal variance with system size denotes partially collective regimes. Thus the $\alpha = 1$, and 3 cases represent the Heisenberg limited and standard quantum limited scaling of sensitivity, respectively, while for the intermediate α values there are still significant sensitivity gains beyond the standard quantum limit.

Identification of $(a_Z/L)_*$ from system size scaling exponent p

In Fig 1(b) and (c) we identified the critical $(a_Z/L)_*$ values marked by yellow markers via the scaling of the minimum variance with system size. We now show two examples of how these values are extracted from the scaling of minimal variance, $\text{Var}[\mathcal{O}^-]_{\min} \sim N^p$ in Fig. S2, which shows the extracted scaling exponent p . The advent of system size scaling at a critical $(a_Z/L)_*$ where p jumps from zero to a nonzero value is clearly visible.

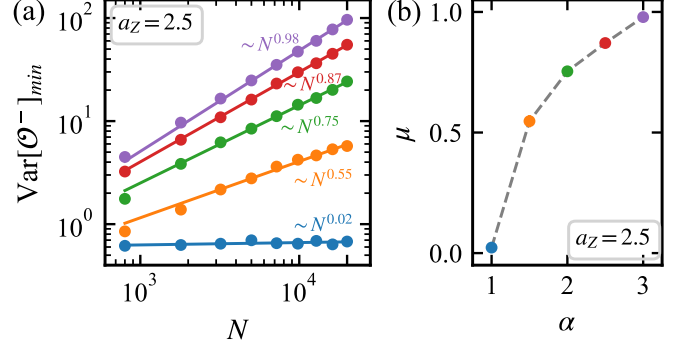


FIG. S1. Scaling of squeezing at fixed layer separation. (a) Scaling of minimal variance with system size for the $2d$ case at fixed layer separation $a_Z = 2.5$ for different interaction exponents α . Solid lines are fits to the function, $\text{Var}[\mathcal{O}^-]_{\min} \sim N^\mu$. (b) Change in scaling exponent μ for different α , showing a fully collective regime ($\mu \approx 0$) for $\alpha = 1$ and non-collective regime ($\mu \approx 1$) for $\alpha = 3$, while a partially collective regime ($0 < \mu < 1$) is seen for intermediate values of α .

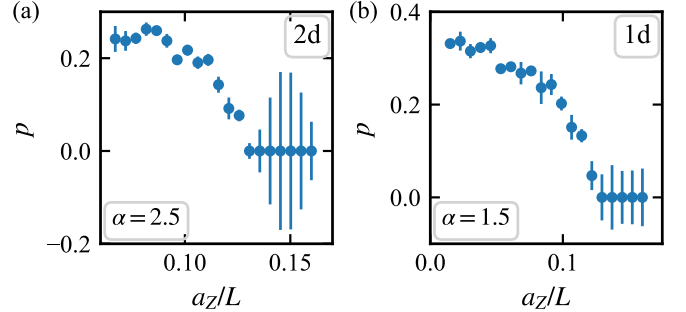


FIG. S2. minimal variance system size scaling exponent p versus a_Z/L for (a) $2d$ and (b) $1d$ cases, where $\text{Var}[\mathcal{O}^-]_{\min} \sim N^p$. p jumps from zero to a nonzero value at the critical a_Z/L_* .

Scaling of variance minima

In the main text, we show the scaling of variance minima for the representative case of $\alpha = 3$ for $2d$ system. We now show the same for the rest of the power-law exponents α in $2d$ systems, as well as for all the α in $1d$ systems in Fig. S4 and Fig. S3, respectively. In all cases, under the rescaling $\text{Var}[\mathcal{O}^-]_{\min}/L^{p \times d}$ the data collapses to a single curve, or scaling function, demonstrating that the aspect ratio a_Z/L controls the transition, and that both distinct regimes show universal scaling of the mini-

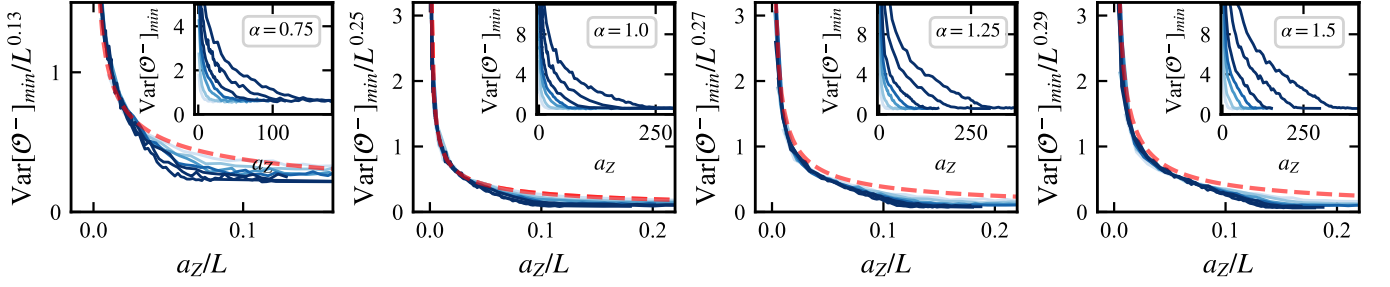


FIG. S3. Universal scaling collapse of minimal squeezing. Inset: Dependence of minimal variance $\text{Var}[\mathcal{O}^-]_{\min}$ on layer spacing a_z , for different system sizes ($L = 100$ to 2500) for $\alpha = 0.75, 1, 1.25,$ and 1.5 in $1d$. Main panel: Rescaled minimal variance $\text{Var}[\mathcal{O}^-]_{\min}/L^{p \times d}$ versus aspect ratio a_z/L for the same system sizes, demonstrating a collapse onto a single curve. The red dashed lines $(a_z/L)^{d_V}$ show fit to the scaling function with d_V from Table. S3

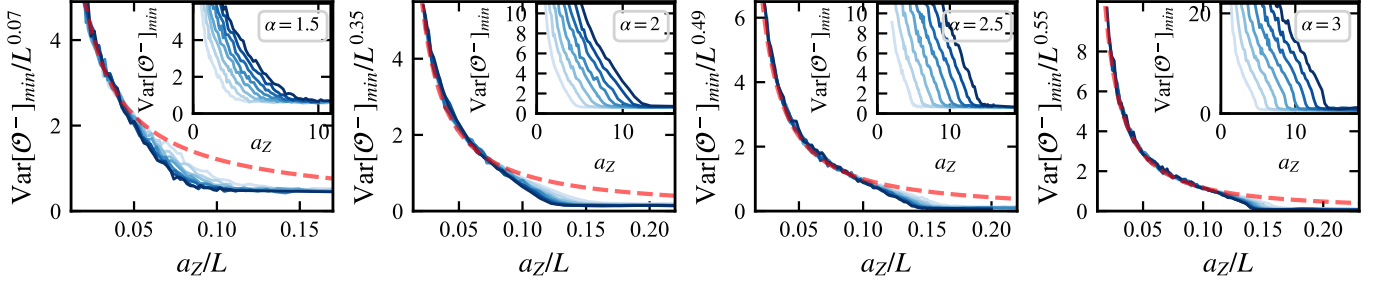


FIG. S4. Universal scaling collapse of minimal squeezing. Inset: Dependence of minimal variance $\text{Var}[\mathcal{O}^-]_{\min}$ on layer spacing a_z , for different system sizes ($L = 30$ to 100) for $\alpha = 1.5, 2,$ and 2.5 in $2d$. Main panel: Rescaled minimal variance $\text{Var}[\mathcal{O}^-]_{\min}/L^{p \times d}$ versus aspect ratio a_z/L for the same system sizes, demonstrating a collapse onto a single curve. The red dashed lines $(a_z/L)^{d_V}$ show fit to the scaling function with d_V from Table. S3

mal variance. Further, while finite size discrepancies near the critical value $(a_z/L)_*$ are visible for smaller L , these are seen to vanish with increasing L . The red dashed line $(a_z/L)^{d_V}$ is an excellent fit to the scaling function.

Determining critical exponents

To derive the exponents and associated uncertainties we follow the procedure proposed in Ref. [65] of the main text, which defines a cost function to assess the best scaling collapse of the data. We first give a general description of the method, before describing its application to our work. We denote arbitrary ‘raw’ data $\{y_{ij}, x_{ij}\}$ for the j ’th point in the i ’th data set (a given system size $N_i = L_i^d$). The data is ordered in increasing system size $\{N_1, N_2, \dots\}$. Consider the scaled data $\{\tilde{x}_{ij}, \tilde{y}_{ij}\} = \{x_{ij}N_i^{d_x}, y_{ij}N_i^{d_y}\}$, for some exponents d_x and d_y . Similarly, we define rescaled uncertainties $\{\tilde{\delta}_{ij}\} = \{\delta_{ij}N_i^{d_y}\}$. If the scaling collapse is successful, we expect \tilde{y}_{ij} to be similar across different data sets for the same \tilde{x}_{ij} values. In general however, such a comparison is difficult as different data sets will not have identical values of \tilde{x}_{ij} . We therefore use linear interpolation to generate curves $f_i(x)$ and $\delta_i(x)$ corresponding to \tilde{y}_{ij} and $\tilde{\delta}_{ij}$, respectively, over a fine spatial grid x . To assess the

success of the scaling collapse, we define the cost function [65]

$$\lambda(d_x, d_y) = \frac{1}{\mathcal{N}} \sum_{i < k} \sum_x \frac{(f_i(x) - f_k(x))^2}{\delta_i(x)^2 + \delta_k(x)^2}, \quad (\text{S1})$$

where the summation x is over the entire (equally spaced) spatial grid for which data sets i and k both exist, and \mathcal{N} is the total number of terms in the summations. The optimal value for the exponent is given by that which minimizes the cost function. While a good collapse is indicated by $\lambda_{\min} \leq 2$, a poor collapse should have a much larger cost function [66]. The exponent’s uncertainty is then extracted from the range of values for d_x and d_y that give $\lambda(d_x, d_y) \leq \lambda_{\min} + 1$ [66], where λ_{\min} is the minimum of the cost function. This amounts to finding the range of exponents for which the cost function is within standard error of the minimum cost function.

Throughout this analysis, we estimate the uncertainty δ_{ij} from the standard error of truncated Wigner samples. Intuitively, calculations within the collective manifold are expected to have less uncertainty. In general, we find that the error scales proportional to $\text{Var}[\mathcal{O}^-]_{\min}$ for a fixed system size. We estimate the numerical error for all α from the $\alpha = 3$ calculation, which yields $\delta \approx 0.04 \text{Var}[\mathcal{O}^-]_{\min}$. This is the most non-collective system we consider in $2d$ and therefore represents a ‘worst-

(a)

α	d_x	Δd_x	λ_{\min}
0.75	-0.88	0.11	0.95
1	-0.9	0.08	1.83
1.25	-0.92	0.05	0.95
1.5	-0.93	0.04	0.37
2	-0.97	0.04	1.78

(b)

α	d_x	Δd_x	λ_{\min}
1.5	-0.8	0.26	0.92
2	-0.9	0.18	1.19
2.5	-0.87	0.11	0.78
3	-0.89	0.17	0.60

TABLE S1. Exponents d_x , uncertainties Δd_x , and minimum cost functions in (a) $1d$ and (b) $2d$.

case' error. We have checked some specific cases explicitly to confirm that this bounds the error for $\alpha < 3$, and that the error scales comparably in $1d$. When evaluating Eq. S1, we typically ignore small system sizes, such as $L < 200$ in $1d$ and $L < 30$ in $2d$, which are not expected to conform to the scaling hypothesis due to larger finite size effects.

We use the results in Fig. 1 as a guide for selecting the appropriate range of a_z/L , which implies a cutoff for a_z at a given L . We also need to avoid the range of a_z values between the collective and partially-collective phases. This is clearly visible in Fig. 2 of the main text where the data starts to deviated from the dotted (red) line. We therefore consider a range of a_z/L that is well inside the phase boundary indicated by Fig. 1.

Scaling of critical a_z with L

We now apply this procedure to estimate the scaling of the critical a_z value, a_z^* , with L . We define the rescaled data $\{\tilde{x}_{ij}, \tilde{y}_{ij}\} = \{(a_z)_j L_i^{d_x}, (\text{Var}[\mathcal{O}^-]_{\min})_{ij}\}$ and only consider data with variance values in the range $\text{Var}[\mathcal{O}^-]_{\min} \lesssim \mathcal{O}(1)$ and a_z values in the vicinity of the transition. Tables S1 summarizes the results. Fig. S5 shows the rescaled data for the optimal d_x value in the case of $\alpha = 2.5$ in $2d$. In $1d$, where we have access to large system sizes, we find $d_x \in \{0.88, 0.97\}$ in all cases, consistent with $d_x = 1$ on the order of the uncertainty. The results are also broadly compatible with $a_z^* \sim L$ for the $2d$ case, although the uncertainty is larger. This justifies the use of a_z/L as the parameter controlling the phase and distance from the critical point in the main text. Larger deviations from $d_x = 1$ in $2d$ may be due to

(a)

α	p	Δp	$\lambda_{\min}^{(p)}$
0.75	0.13	0.06	0.89
1	0.25	0.06	1.30
1.25	0.27	0.06	0.96
1.5	0.29	0.06	1.49
2	0.35	0.05	0.57

(b)

α	p	Δp	$\lambda_{\min}^{(p)}$
1.5	0.035	0.055	0.50
2	0.175	0.055	0.63
2.5	0.245	0.065	0.48
3	0.275	0.065	0.61

TABLE S2. Exponents p , uncertainties Δp , and minimum cost functions in (a) $1d$ and (b) $2d$, estimated from the minimum variance data (as in Fig. 2 of the main text).

enhanced finite size effects.

Estimating exponent p from variance minima.

In this section we estimate the exponent p , where $\text{Var}[\mathcal{O}^-]N^{-p} = y(a_z/L)$, from the variance minima data. In this instance the optimization is only carried out for a single exponent which scales the y-data. We apply the aforementioned optimization procedure with $\{\tilde{x}_{ij}, \tilde{y}_{ij}\} = \{(a_z)_j/L_i, (\text{Var}[\mathcal{O}^-]_{\min})_{ij}N_i^{-p}\}$. To restrict the data to the partially collective phase, we only consider data for which $\text{Var}[\mathcal{O}^-]_{\min}$ is c times greater than its value in the collective phase, i.e. $\text{Var}[\mathcal{O}^-]_{\min} > c \lim_{a_z \rightarrow \infty} \text{Var}[\mathcal{O}^-]_{\min}$, where the limit is estimated by averaging over the variance in the collective phase. Typically we choose c to be between 4 and 10, depending on α . The results are listed in Table S2. Using these p exponents, in Fig. 2 of main text, as well as in Figs. S3 and S4, we plot $\text{Var}[\mathcal{O}^-]_{\min}L^{-pd}$ versus aspect ratio a_z/L for different system size. The data in the partially collective phase collapses onto a single curve in all cases. Furthermore, the scaling function in this region is well described by $\text{Var}[\mathcal{O}^-]_{\min}L^{-pd} = (a_z/L)^{d_V}$, where d_V is estimated in the subsequent section.

Estimating exponents d_V, d_τ, ν, δ .

We now discuss the estimation of the four exponents d_V, d_τ, ν, δ . Since p has already been computed, we use $p = d_V(1-\delta)/d + \nu$ to constrain ν and reduce the number of unknowns to three (d_V, d_τ, δ).

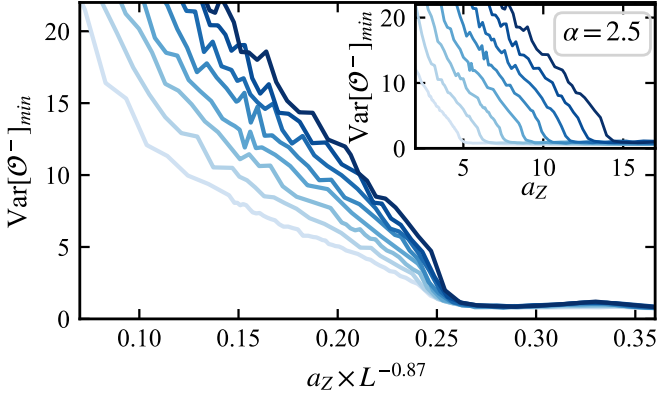


FIG. S5. Scaling collapse of the critical a_z value (a_z^*) vs L . Inset: Dependence of minimal variance $\text{Var}[\mathcal{O}^-]_{\min}$ on layer spacing a_z , for different system sizes ($L = 30$ to 100) with $\alpha = 2.5$ in $2d$. The opacity increases with system size. Main panel: $\text{Var}[\mathcal{O}^-]_{\min}$ vs $a_z L^{-0.87}$, demonstrating a collapse of the critical values $a_z^* L^{-0.87}$ to approximately a single point.

The exponents d_V and d_τ are estimated simultaneously from the data for the largest available system size at a given α : typically $N = 2500$ in $1d$ and $N = 10000$ ($L = 100$) in $2d$. As discussed, and shown in Fig. 4(a) of the main text, this obeys the relation $\text{Var}[\mathcal{O}^-] a_z^{-d_V} = f_N[(t - t_{\min}) a_z^{-d_\tau}]$. We therefore apply the optimization procedure over a two dimensional grid of $\{d_V, d_\tau\}$ values using $\{\tilde{x}_{ij}, \tilde{y}_{ij}\} = \{(t - t_{\min})_j (a_z)_i^{-d_\tau}, (\text{Var}[\mathcal{O}^-]_{\min})_{ij} (a_z)_i^{-d_V}\}$. The results are shown in Table S3. Fig. S6 (1d) and Fig. S7 (2d) include plots of $\text{Var}[\mathcal{O}^-] a_z^{-d_V}$ vs $(t - t_{\min}) a_z^{-d_\tau}$ for different a_z values, as well as the corresponding raw data (inset). Data is only plotted over the range of a_z values that are used to extract the exponents.

Since the critical point occurs at finite $a_z/L =$ constant, it is difficult to access a large range of a_z values in $2d$. This issue is also exacerbated for lower α (even in $1d$) where this constant is reduced, as shown by the phase boundary in Fig. 1(a) of the main text. In these cases the range of a_z values in the partially collective phase that we can access becomes small, and our results are less substantive. Nevertheless, we include these results for completeness. The reduced data range is reflected in larger relative uncertainties $\Delta d_V/d_V$ and $\Delta d_\tau/d_\tau$ for these cases. Note that we are still able to simulate a significant range of N values in these cases, since $N = L^2$, which allows us to obtain reasonable estimates for the exponents p and δ .

To estimate δ we would like to consider a similar procedure for the full scaling function in Eq. 2. To make the problem computationally tractable we assume the optimal values for d_τ , d_V and p . In this case the data is three dimensional and we use t_j to

index time, $(a_z)_i$ for the layer spacing and N_k for the system size. We therefore define $\{\tilde{x}_{ijk}, \tilde{y}_{ijk}\} = \{(t - t_{\min})_j (a_z)_i^{-d_\tau} N_k^{\delta d_\tau/d}, (\text{Var}[\mathcal{O}^-]_{\min})_{ij} (a_z)_i^{-d_V} N_k^{d_V \delta/d - \nu}\}$. The cost-function in Eq. S1 is adapted to include a summation over the system size index, in addition to summing over rescaled time and all $(a_z)_i$ curves. The cost-function is then evaluated for a range of δ , with the results presented in Table S3. Fig. S6 (1d) and Fig. S7 (2d) include plots of $\text{Var}[\mathcal{O}^-] a_z^{-d_V} N^{d_V \delta/d - \nu}$ vs $(t - t_{\min}) a_z^{-d_\tau} N^{\delta d_\tau/d}$ for different N and a_z values. While the data typically does not conform to the criterion for a good fit $\lambda_{\min} \leq 2$, it is also generally not a poor fit, as would be indicated by a very large cost function $\lambda_{\min} \gg \mathcal{O}(1)$. In general, we find that the cost functions can be reduced by considering a_z/L values that are slightly further away from the transition. This lessens the impact of the cross-over region between the partially collective and collective regimes. However, this comes with the trade-off of reducing the range of data that can be considered, which tends to increase the uncertainty. Future works could improve on this by reaching larger system sizes, thereby expanding the range of accessible a_z values in the partially collective regime.

Since d_V , d_τ , δ and p are now known we can calculate $\nu = p - d_V(1 - \delta)/d$, with its uncertainty following from error propagation. This is also presented in Table S3. Since this calculation depends on the other exponents and their uncertainties, the uncertainty tends to be larger than in the aforementioned cases.

(a)										
α	d_V	Δd_V	d_τ	Δd_τ	$\lambda_{\min}^{(d_V, d_\tau)}$	δ	$\Delta \delta$	$\lambda_{\min}^{(\delta)}$	ν	$\Delta \nu$
0.75	-0.43	0.16	0.09	0.05	1.11	3.90	0.32	2.96	-1.12	0.63
1	-0.61	0.16	0.25	0.05	3.31	1.07	0.12	3.04	0.21	0.08
1.25	-0.69	0.16	0.43	0.05	2.30	0.46	0.05	2.45	0.64	0.19
1.5	-0.69	0.2	0.63	0.07	1.72	0.25	0.04	2.11	0.81	0.29
(b)										
α	d_V	Δd_V	d_τ	Δd_τ	$\lambda_{\min}^{(d_V, d_\tau)}$	δ	$\Delta \delta$	$\lambda_{\min}^{(\delta)}$	ν	$\Delta \nu$
1.5	-0.88	0.34	0.16	0.08	1.14	4.2	0.3	6.00	-1.37	0.70
2	-1.11	0.22	0.38	0.06	2.24	1.06	0.16	2.39	0.14	0.07
2.5	-1.22	0.22	0.7	0.08	1.27	0.34	0.08	1.19	0.65	0.23
3	-1.29	0.22	1.12	0.08	2.20	0.15	0.06	2.14	0.82	0.38

TABLE S3. Exponents d_V , d_τ , δ , ν alongside their respective uncertainties, and the corresponding minimum cost functions $\lambda_{\min}^{(d_V, d_\tau)}$ and $\lambda_{\min}^{(\delta)}$ respectively. Data corresponds to (a) $1d$ and (b) $2d$.

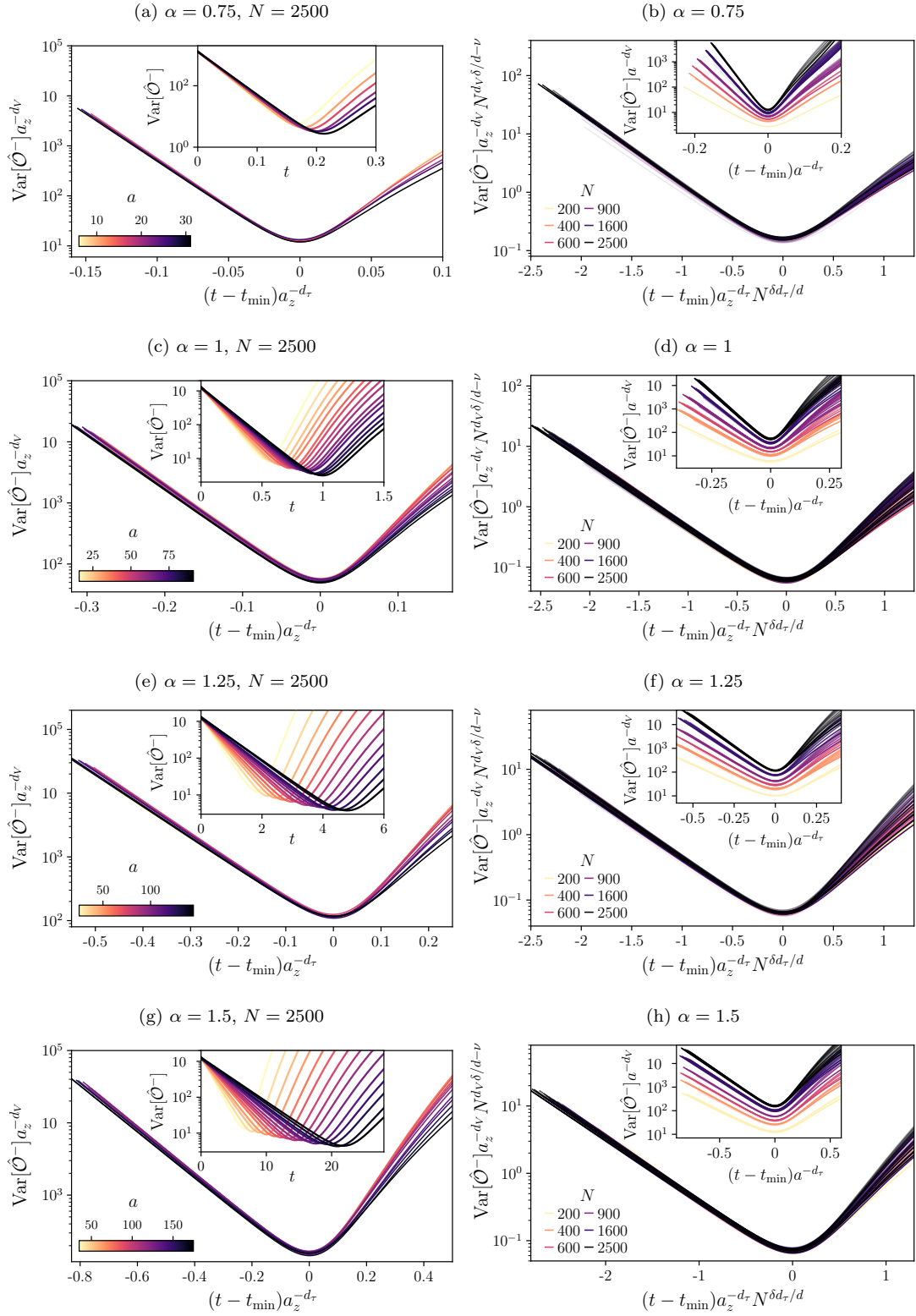


FIG. S6. Raw data and scaling collapses for different α in $1d$, analogous to Fig. 4 of the main text albeit only plotting data that is used to extract the exponents.

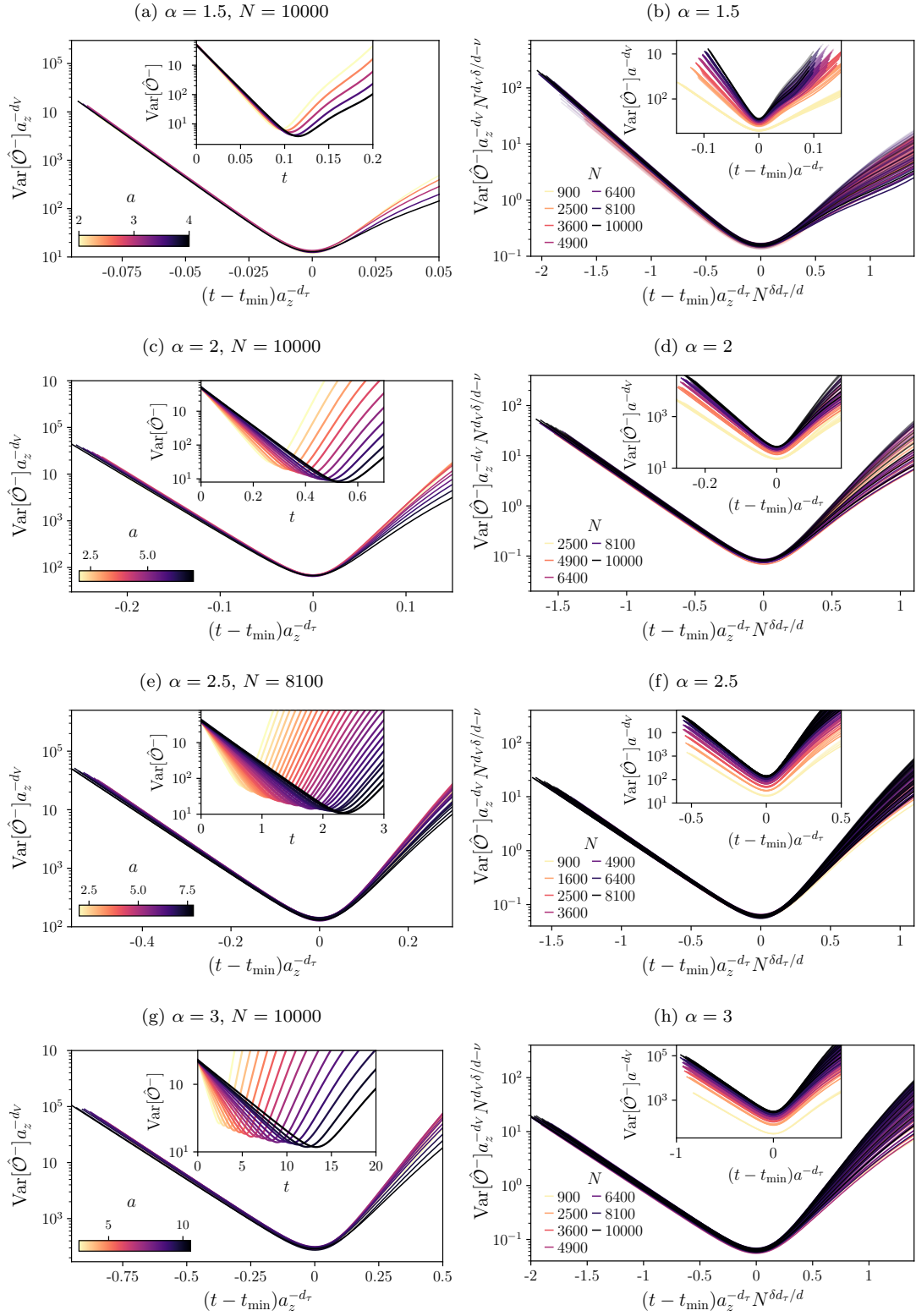


FIG. S7. Raw data and scaling collapses for different α in $2d$, analogous to Fig. 4 of the main text.